X-RAY SPECTROMETRY
X-Ray Spectrom. **28**, 421–426 (1999)

TUTORIAL

Error Factors in Quantitative Total Reflection X-Ray Fluorescence Analysis

Yoshihiro Mori* and Kenichi Uemura
Advanced Technology Research Laboratories, Nippon Steel Corporation, c/o NSC Electron Corporation, 3434 Shimata, Hikari, Yamaguchi 743-0063, Japan

This paper reviews and discusses the error factors in quantitative total reflection x-ray fluorescence analysis, primarily with regard to the surface contamination of silicon wafers. The error factors were classified into three origins: instrumental, sample and data processing. The instrumental error factors originate from source x-ray stability, accuracy of the mechanical glancing angle, position accuracy of sample stage and spurious peaks from the detection system. The sample error factors arise from lateral and depth distribution of the analyte, surface roughness and diffraction of the primary x-rays. The data processing error factors are from interfering peaks and background definition. The accuracy and detection limit are affected by all the error sources listed above. Of these factors, the depth distribution of the analyte is the most important, because this factor is often overlooked and because it is difficult to control.

INTRODUCTION

Total reflection x-ray fluorescence (TXRF) spectrometry is one of the most powerful tools available for analyzing transition metal impurities on the surface of semiconductors.[1] TXRF has come into wide use for daily contamination control in the production of silicon devices. Today, over 300 TXRF instruments are in operation throughout the world. This means that almost all leading-edge semiconductor factories utilize at least one TXRF machine.

While conventional methods such as the atomic absorption spectrometry (AAS)[2] and inductively coupled plasma mass spectrophotometry (ICP-MS)[3] require special expertise for metal extraction and measurement, TXRF needs no sample preparation. For this reason, many individuals who do not possess a particular expertise in analysis use TXRF. However, the use of TXRF involves many factors that can introduce errors, and some error factors are often overlooked. Hence the concentration determined by different analysts using the TXRF method is sometimes different for the same samples or the same data.

The aim of this paper is to review the factors involved in quantitative TXRF measurement that lead to errors. This paper primarily focuses on the analysis of transition metal impurities on silicon wafers, because the principal application of TXRF involves the manufacture of large-scale integrated (LSI) circuits. The factors examined in this paper are concisely listed in Table 1 and are illustrated schematically in Fig. 1. We shall examine these factors one by one.

* Correspondence to: Y. Mori, Advanced Technology Research Laboratories, Nippon Steel Corporation, c/o NSC Electron Corporation, 3434 Shimata, Hikari, Yamaguchi 743-0063, Japan.
E-mail address: mori@re.nsc.co.jp

EXPERIMENTAL

Instrumentation

The TXRF instruments used in this work were a SYSTEM3726B (Rigaku) and a TREX610T (Technos). Each machine was equipped with a rotating anode x-ray source, a multilayer monochromator and an Si(Li) solid-state detector (SSD). In the SYSTEM3726B, the excitation x-ray was Au Lβ (11.44 keV); the applied voltage was 30 kV and the current was 300 mA. In measuring the angular dependence of fluorescence on the SYSTEM3726B, a comb-like absorber made of Pb was placed in front of the monochromator to reduce the intensity of the primary x-rays. The x-ray source of the TREX610T was W Lβ (9.67 keV); the applied voltage was 30 kV and the current was 200 mA.

Sample preparation

The substrates used were polished silicon wafers. For the blanks, the wafers were cleaned with an acidic solution, such as dilute hydrogen fluoride (DHF), hydrogen chloride–hydrogen peroxide mixture (HPM)[4] or hydrogen fluoride–hydrogen peroxide mixture (FPM).[5] Three types of intentionally contaminated sample wafers were examined: spin-coat,[6] immersion in alkaline hydrogen proxide solution (IAP)[7,8] and microdrop.[9]

CCC 0049–8246/99/060421–06 $17.50

Received 7 May 1999
Accepted 30 July 1999

Table 1. Error factors examined in this work

Instrumental factors	
(a) Primary x-ray stability	Accuracy
(b) Accuracy of glancing angle	Accuracy
(c) Position accuracy	Accuracy
(d) Spurious peaks	LLD
Sample factors	
(e) Lateral distribution	Accuracy
(f) Depth distribution	Accuracy
(g) Surface roughness	Accuracy
(h) Diffraction	LLD
Data processing factors	
(i) Interfering peaks	Accuracy
(j) Background definition	LLD

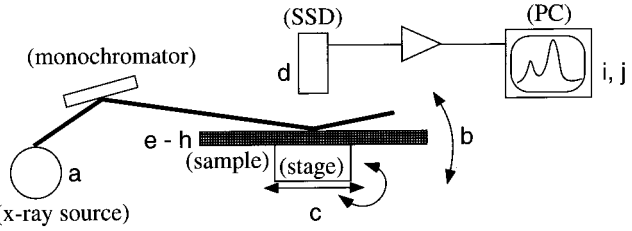

Figure 1. Schematic illustration of the origins of errors examined in this work.

RESULTS AND DISCUSSION

Instrumental factors

Primary X-ray stability. In a fixed optical system, the x-ray fluorescence intensity is proportional to the primary x-ray intensity. Consequently, the stability of the primary x-ray intensity directly affects the determination value. Also, if the fluorescent or reflected x-rays are monitored for the adjustment of the glancing angle, an additional problem occurs. As a means of improving glancing angle reproducibility, recent instruments have an Si Kα normalization mode. In this mode, a representative Si Kα intensity for a typical wafer or typical point on a wafer at a glancing angle is measured and memorized before the analysis is begun. When the analysis begins, adjustment of the glancing angle for a sample is made by driving the stepping motor of the glancing angle axis so that the detected Si Kα intensity equals the memorized value. This method is valid if the primary x-ray intensity is stable. If the primary x-ray intensity is lower than in the initial Si Kα measurement, for example, this function increases the actual glancing angle to equalize the Si Kα intensity, and the sample is measured at a higher glancing angle. The change in the glancing angle causes errors, which will be discussed in the next section.

Accuracy of the glancing angle. Because the surface x-ray intensity and penetration depth of the incident x-rays are functions of the glancing angle,[10] the accuracy of the glancing angle strongly influences the intensity of the fluorescent x-rays from the sample. Figure 2 is an example of the angular dependence of fluorescence for a silicon wafer on which Ni is spin-coated. This figure shows that the x-ray fluorescence intensity is strongly dependent

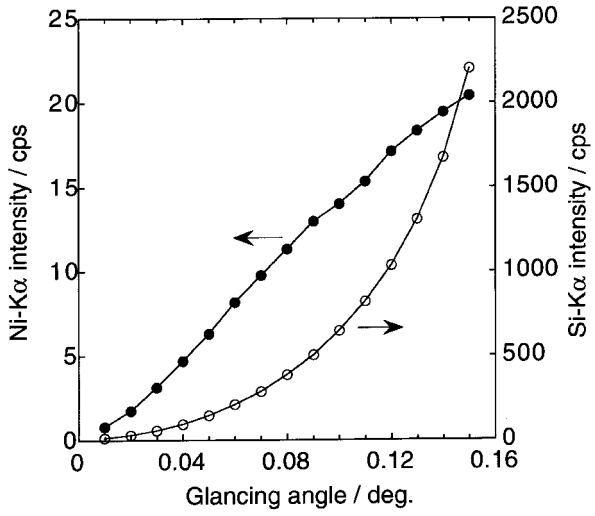

Figure 2. Example of angular dependence of the fluorescence for an Si wafer on which Ni is spin-coated. (○) Si Kα; (●) Ni Kα.

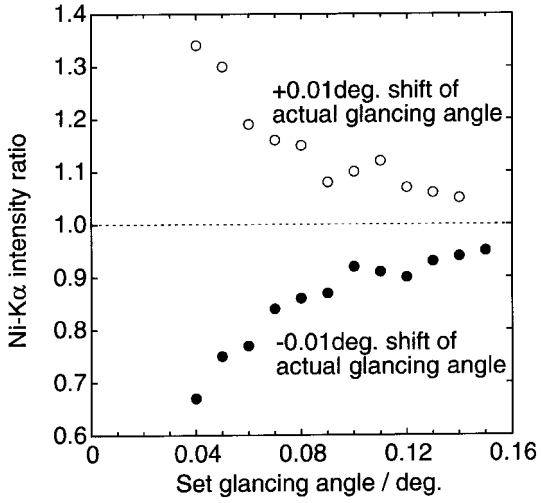

Figure 3. Variation of Ni Kα intensity with a 0.01° shift of the glancing angle from a set point. The open circle represents the relative intensity of Ni Kα when the measuring glancing angle becomes 0.01° higher than the set angle, and the closed circle represents the intensity when the measuring angle is 0.01° smaller.

on the glancing angle. Figure 3 shows the variations of Ni Kα intensity with a 0.01° shift at each glancing angle, which were calculated from the data in Fig. 2. This figure indicates that only a 0.01° shift causes a 10–30% error in fluorescence intensity under the general measuring conditions (0.05–0.10°). To recognize the extent of this error, it is important to know the accuracy of the glancing angle for each instrument. If the primary x-ray intensity is stable enough, the reproducibility of the glancing angle can be monitored with Si Kα.

In some cases, spectra are normalized by the Si Kα intensity to adjust the *y*-axis. This type of normalization involves some errors that originate in the differences of the angular dependence of the fluorescence between Si and the analyte. In Fig. 2, the slopes of Si Kα and Ni Kα are different, meaning that the normalization coefficients of Si Kα and Ni Kα are not the same. Table 2 shows an example of this. For instance, if the data obtained at 0.04° are normalized by the Si Kα at 0.05°, the Ni Kα intensity is

Table 2. Estimated error when the contribution of the glancing angle shift is normalized by the Si Kα intensity

Actual glancing angle (°)	0.03	0.04	0.05	0.06	0.07
Actual Si Kα (cps)	57.11	95.09	146.29	209.66	287.74
Actual Ni Kα (cps)	3.13	4.70	6.29	8.17	9.75
Ni Kα normalized by Si Kα at 0.05° (cps)	8.02	7.23	6.29	5.70	4.95
Estimated error (%)	+28	+15	0	−9	−21

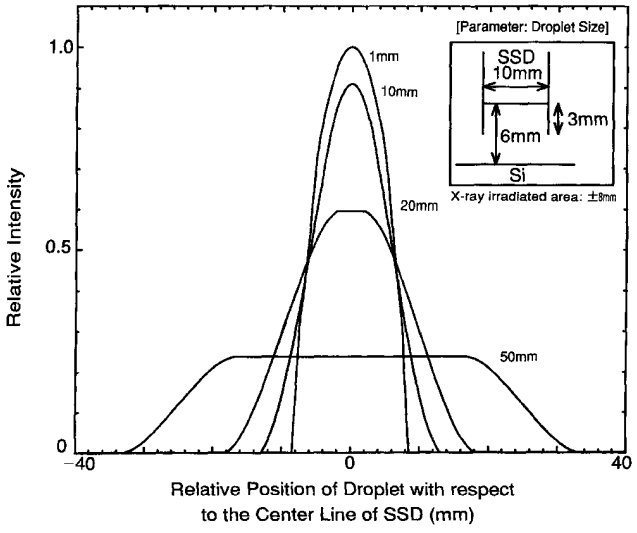

Figure 4. Calculated dependence of detection position on fluorescence from several diameters of analyte.[11]

calculated as 7.23 cps, although the actual Ni Kα at 0.05° should be 6.29 cps. In this case, the error is +15%. From this example, it is obvious that the normalization of the Si Kα intensity is not appropriate for quantitative TXRF.

Position accuracy. Figure 4 shows the calculated detection position dependence of fluorescence for several diameters of analyte.[11] This figure indicates that the fluorescence intensity depends on the lateral distance between the detector and the analyte. The variation becomes more critical if the analyte is concentrated in a small area. If the area is very small (<10 mm in diameter), a shift of a few millimeters in the detection position causes a serious error in quantification. When a sample wafer is loaded without automatic positioning, it may be inaccurate by a few millimeters. Wafer positioning is critical if the analyte is concentrated in a small area. The latest instruments are equipped with automatic wafer positioning mechanisms that employ optical sensors, so most of the above-mentioned errors can be avoided. This problem is the primary one to consider if older instruments are used.

Spurious peaks. The detection of total reflection x-ray fluorescence is one of the most critical applications for an Si(Li) SSD. Thus, a new problem that originates in detector quality is revealed: that of the spurious peak (or impurity peak).[12,13] Any impurities in the detection element or casing are excited by scattered or diffracted excitation x-rays, and emit their characteristic fluorescent x-rays. These x-rays are detected by the SSD, and spurious peaks appear in the measured spectrum. Figure 5 is a sample spectrum

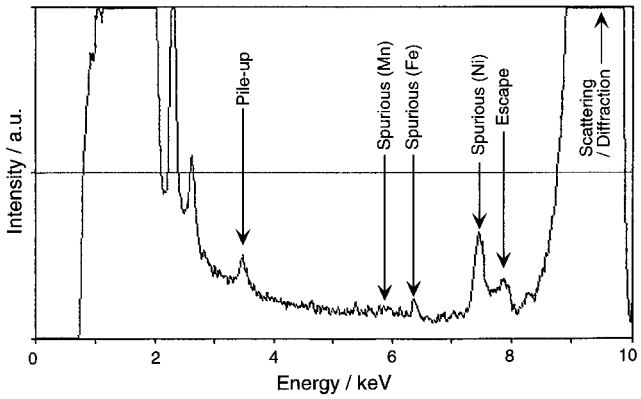

Figure 5. Sample spectrum showing spurious peaks and interfering peaks.

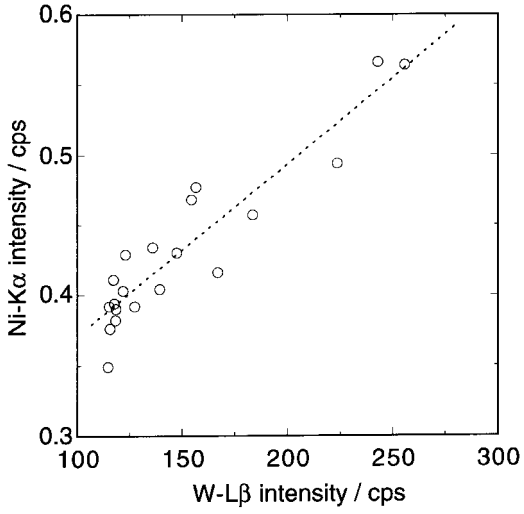

Figure 6. Sample relationship between spurious Ni Kα and excitation W Lβ.

in which spurious peaks of Mn, Fe and Ni are observed. Some researchers have reported spurious peaks of other elements such as Cu.[14] Because of their origin, the intensity of the spurious peaks is proportional to the intensity of the excitation x-ray that strikes the SSD. The proportionality coefficients for different detectors are not the same. Figure 6 is an example of this relationship for Ni. By using the coefficients determined at the time of shipment from the factory, recent software subtracts the contribution of spurious peaks from the spectrum or from the integrated intensity. This means that most TXRF users are not aware of the existence of these peaks. However, the peaks affect the lower limit of detection (LLD) as follows.

From the perspective of the x-ray detection system, the statistical variation of fluorescence intensity is proportional to the square root of signal intensity, and the LLD is proportional to the statistical variation. Here the LLD is defined as

$$\mathrm{LLD} = 3{I_{\mathrm{BG}}}^{1/2}S \qquad (1)$$

where I_{BG} is the background intensity (signal intensity of a blank sample) and S is the slope of the calibration curve.[15] Therefore, any spurious peak is included in I_{BG}, and the statistical variation (${I_{\mathrm{BG}}}^{1/2}$) increases, followed by deterioration of the LLD. For example, for the instrument in Fig. 5, the LLD of Ni is calculated to be 2×10^9 atoms cm^{-2}

if the contribution of spurious peaks is subtracted, and it becomes 5×10^9 atoms cm^{-2} if the entire signal of the blank sample is used. Although the contribution of any spurious peaks is usually subtracted when calculating I_{BG}, this is incorrect because of the above reason as for LLD calculation. The LLD should be determined under conditions so that the contribution of any spurious peaks is not subtracted.

Sample factors

Lateral distribution. In Fig. 4, the total amount of analyte is kept the same for all calculations. It can then be assumed that the fluorescence intensity depends on the size of the segregated area, even if the wafer positioning is perfect. For accurate determination, calibration standard samples that have the same segregated area as the unknown sample must be prepared. This factor is especially critical for concentrating methods such as vapor phase decomposition (VPD)–TXRF.[16] In such a preconcentration technique, the drying process must be carefully controlled to equate the size of the concentrated areas among the samples.[11]

Depth distribution. It is well known that TXRF is sensitive to the depth profile of the analyte. This presents a very serious problem in quantitative analysis. An example to explain this error factor is shown in Fig. 7. This figure shows the changes in the angular dependence of fluorescence for a Cu-contaminated silicon wafer (1.0×10^{13} atoms cm^{-2} by AAS) over time.[17] Since the diffusion coefficient of Cu in Si is very large,[18] the depth distribution of Cu changes as a function of time after the adsorption. This figure can be regarded as the angular dependence of fluorescence for different samples that have the same concentration. Here, suppose that a TXRF instrument is calibrated with sample A at a glancing angle of 0.05°. Then samples B and D are quantified as 0.8×10^{13} and 0.5×10^{13} atoms cm^{-2}, respectively, although these samples have identical concentrations. This degree of error can easily occur through the differences in depth profiles between a standard wafer and an unknown sample.

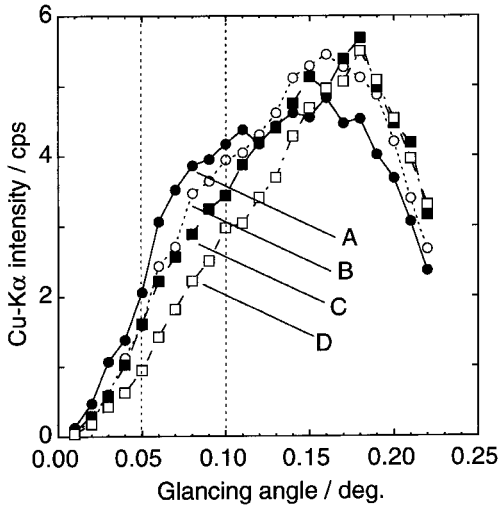

Figure 7. Change of angular dependence of the fluorescence for a Cu-contaminated silicon wafer over time. The contamination concentration is 1.0×10^{13} atoms cm^{-2} by AAS. (A) 6 h; (B) 29 h; (C) 71 h; (D) 163 h after the contamination.

Figure 7 also suggests another type of error caused by the differences of measurement glancing angle. Suppose that two laboratories, Y and Z, calibrate their TXRF instruments with sample A and their measurement glancing angles are 0.05° and 0.10° deg., respectively. When Y and Z measure unknown sample D, they quantify it as 0.5×10^{13} and 0.7×10^{13} atoms cm^{-2}, respectively, although they used the same standard sample. This is because the fluorescence intensity ratios of sample A to sample D depend on the glancing angle. In other words, the differences are caused because their angular dependences of fluorescence are not geometrically similar. Using the same standard samples for different TXRF instruments does not always guarantee accuracy of quantification if the measurement glancing angles are different.

This factor is often overlooked or is not considered, because it is difficult to know the depth distribution of the analyte before measurement. In our experience, this factor is the prime reason for disagreements between values determined by AAS and TXRF and between those determined using different TXRF instruments.

Surface roughness. Figure 8 shows the angular dependence of fluorescence for surface impurities on smooth and rough surfaces.[19] The surface roughness flattens the profile of angular dependence, causing the same type of error discussed in the Depth distribution section.

Diffraction. Because a silicon wafer is a single crystal, diffraction of incident x-rays occurs under certain conditions. For W Lβ (9.67 keV) into a Si (100) surface, the incidence of $[110] \pm 90N^\circ$ and $[110] \pm 25 \pm 90N^\circ$ (where N is an integer) gives a large diffraction peak in the spectrum.[20] The large W Lβ peak causes two problems: spurious peaks and background enhancement. The former problem was already discussed in the Instrumental

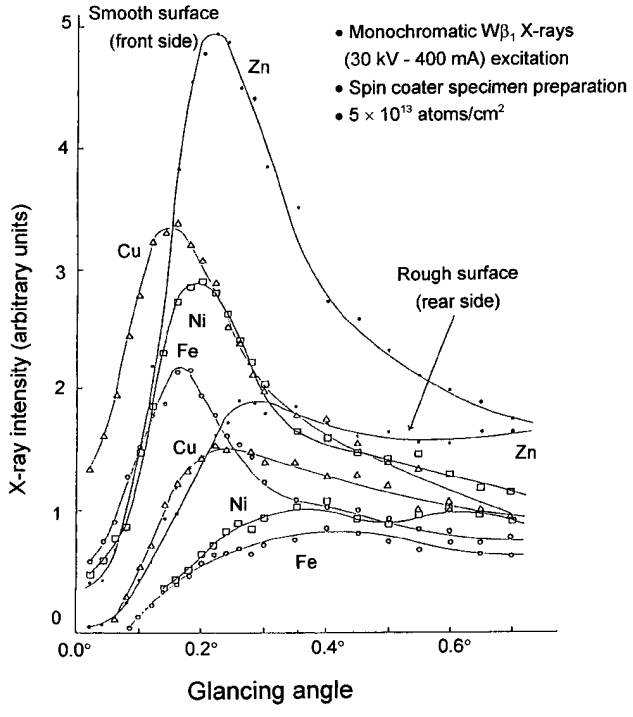

Figure 8. Example of angular dependence of fluorescence for the surface impurities on mirror and rough surfaces.[19]

factors section. A large W Lβ gives larger spurious peaks, causing deterioration of the LLD. The latter issue, background enhancement, also concerns the LLD. When the diffraction causes the W Lβ intensity to be very high, the background of the transition metal peaks becomes high because of the tailing of W Lβ. The value of LLD depends on the background intensity, as is described in Eqn (1), so the higher background level deteriorates the LLD. To avoid this problem, the analyst must set the azimuth angle so that diffraction does not occur. However, if the sample stage is $r-\theta$ controlled, the azimuth angle (θ) is automatically determined when a certain measurement position is selected, and it is impossible to choose θ. Hence the LLDs vary within the points as for mapping measurement, and the best LLD is not always achieved on an $r-\theta$ stage. To resolve the above problem, an $x-y-\theta$-controlled sample stage was developed, and its merits were verified.[21]

Data processing factors

Treatment of interfering peaks. In TXRF spectra, there are three types of interfering peaks: scattered incident x-rays, escape peak and pile-up peak (Fig. 5). These peaks partly overlap the actual fluorescence peaks.

Most commercial TXRF instruments use W Lβ x-ray for excitation. The incident W Lβ x-rays are scattered on the sample surface, producing a large peak in the spectrum. Although the characteristic energy of W Lβ (9.67 keV) is separated from that of Zn Kα (8.63 keV), the tail of W Lβ overlaps Zn Kα so that it acts as an interfering peak. Figures 9 and 10 show the sample spectra obtained on different instruments. The quantification results for both instruments are 'below the detection limit,' while their peaks are visible to the eye. These results show the limit of peak separation between a large W Lβ and a small Zn Kα. Careful treatment and interpretation are needed for low concentrations of Zn.

When the scattered or diffracted W Lβ strikes the detector, part of its energy is absorbed by the Si(Li) detector and the remainder appears as an escape peak. The energy of the escape peak in this case, 7.93 keV, corresponds to the energy difference of W Lβ (9.67 keV) and Si Kα (1.74 keV). This peak overlaps Cu Kα (8.04 keV) and interferes with the determination of Cu. Because of the origin, the intensity of the escape peak is proportional to the W Lβ intensity, as is shown in Fig. 11. In some recent data processing programs, the peak is subtracted by using this relationship. However, the existence of escape peak deteriorates the LLD whether its contribution is compensated for or not, as discussed in the Spurious peaks section. Also, in some cases, peak separation is performed between Cu Kα and the escape peak. However, this separation is very difficult to handle, for two reasons: (1) the energy difference of the two peaks (0.11 keV) is smaller than the energy resolution of the SSD (typically 0.17 keV as full width at half-maximum around 8 keV) so that the overlap area is large and (2) the intensity of the escape peak is often too small to make a best fit as a Gaussian peak.

Newer instruments have a high-power x-ray source to improve detection limits. However, the greater the excitation x-ray intensity, the more difficult the treatment of the two interfering peaks becomes, because their intensity is directly proportional to the W Lβ intensity. W Lβ

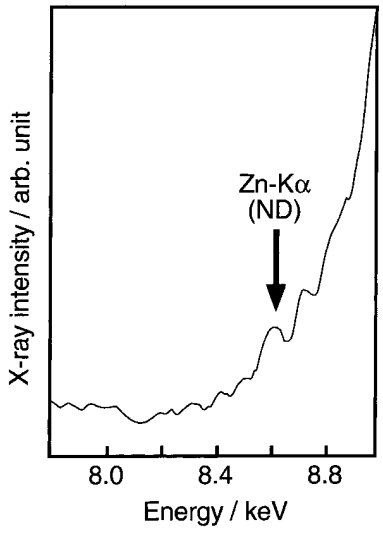

Figure 9. Sample spectrum relative to the overlap of W Lβ and Zn Kα (1).

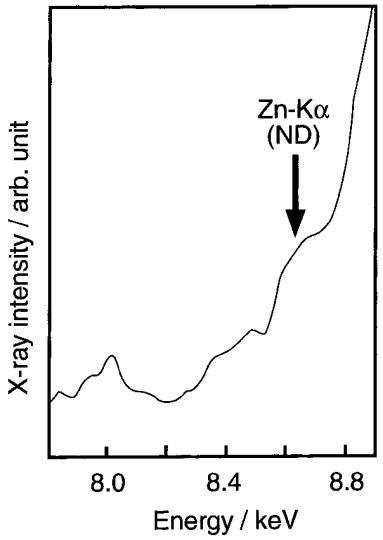

Figure 10. Sample spectrum relative to the overlap of W Lβ and Zn Kα (2).

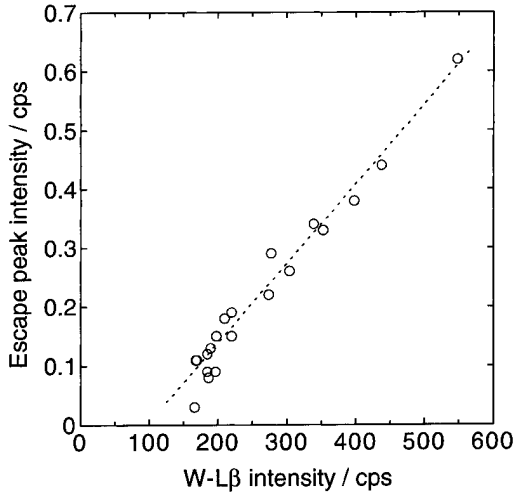

Figure 11. Sample relationship between escape peak and excitation W Lβ.

excitation has these inherent limits when used in an attempt to improve the detection limits by increasing the intensity of the excitation x-rays. Other x-ray sources, such as Au Lβ,[22] are effective in avoiding these problems.

The third interfering peak is the so-called 'pile-up' peak. Because the multichannel analyzer (MCA) cannot distinguish between the photons coming in at the same time, a pile-up peak appears at the sum of the energies of two photons. The generation of a pile-up peak is influenced by the probability of simultaneous incidence, and this probability is very low. However, high-intensity x-rays sometimes generate a distinguishable pile-up peak. In Si wafer analysis, Si Kα (1.74 keV) can generate a pile-up peak at 3.48 keV, which is the sum of two Si Kα photons. This pile-up peak is adjacent to K Kα (3.31 keV) and Ca Kα (3.69 keV), and interferes with their quantification. The energy differences, 0.17 and 0.21 keV, are larger than the energy resolution of the SSD, so the peak separation is easier to handle than the case of Cu Kα versus the escape peak mentioned above.

Background definition. The x-ray fluorescence spectrum from an element can be divided to two parts: the net signal of the analyte and the background signal. The background signal is defined as the area of the spectrum below the baseline within a certain energy region of interest (ROI). Although this definition seems to be strict, it actually involves ambiguity. When an attempt is made to calculate the background intensity, a certain ROI must be defined. The ROI definition is different for each data processing program. This affects the value of the LLD, because the LLD depends on the background intensity [see Eqn (1)]. For example, the spectrum shown in Fig. 12 was actually processed with two different programs, and the output background intensities of Ni Kα were not the same: software A gave 0.89 cps whereas software B gave 0.62 cps. The LLD of software A is then calculated to be 1.2 ($= 0.89^{1/2}/0.62^{1/2}$) times larger than that of software B, although the given spectra are identical. This introduces differences in deciding about the existence of trace amounts of impurities near the LLD level. Standardization of background definition is required for impartiality.

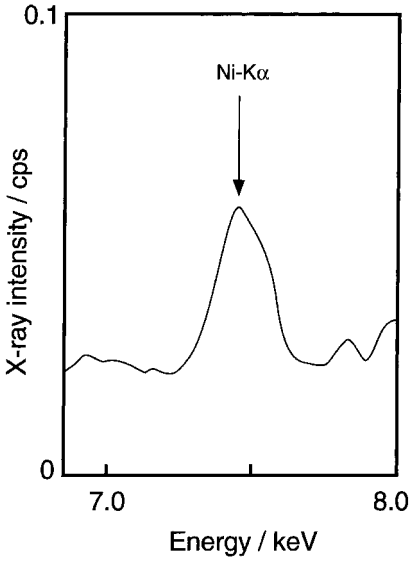

Figure 12. Sample spectrum used for the examination of background definition.

CONCLUSION

This paper has presented many factors that can cause errors in quantitative TXRF. The factors are categorized into three groups: instrumental, sample characteristics and data processing. We believe that almost all factors have an influence on all TXRF instruments. Although some official standardization of TXRF measurements have been made or is in progress,[15] not all factors are being considered. Actually, some factors are impossible to standardize because of practical difficulties. Analysts must always take these factors into careful consideration when using TXRF for quantitative analysis.

REFERENCES

1. R. S. Hockett, *Adv. X-Ray Anal.* **37**, 565 (1994).
2. A. Shimazaki, H. Hiratsuka, Y. Matsushita and S. Shoji, in *Extended Abstracts of the 16th (1984 International) Conference on Solid State Devices and Materials, Kobe*, p. 281, (1984).
3. M. Takenaka, M. Tomita, A. Kubota, N. Tsuchiya and H. Matsunaga, *Bunseki Kagaku* **43**, 169 (1994).
4. W. Kern and D. A. Puotinen, *RCA Rev.* **31**, 187 (1970).
5. T. Shimono and M. Tsuji, in *Extended Abstracts of the 179th Electrochemical Society Meeting, Washington, DC*, ECS Proceedings, Vol. PV91-1, p. 278 (1991).
6. M. Hourai, T. Naridomi, Y. Oka, K. Murakami, S. Sumita, N. Fujino and T. Shiraiwa, *Jpn. J. Appl. Phys.* **27**, L2361 (1988).
7. Y. Mori, K. Shimanoe and T. Sakon, *Anal. Sci.* **11**, 499 (1995).
8. Y. Mori and K. Shimanoe, *Anal. Sci.* **12**, 141 (1996).
9. H. Kondo, J. Ryuta, E. Morita, T. Yoshimi and Y. Shimanuki, *Jpn. J. Appl. Phys.* **31**, L11 (1992).
10. A. Iida, A. Yoshinaga and Y. Gohshi, *Anal. Chem.* **58**, 394 (1986).
11. K. Yakushiji, S. Ohkawa and A. Yoshinaga, *Adv. X-Ray Chem. Anal. Jpn.* **24**, 87 (1993).
12. K. Yakushiji, S. Ohkawa, A. Yoshinaga and J. Harada, *Jpn. J. Appl. Phys.* **31**, 2872 (1992).
13. K. Yakushiji, S. Ohkawa, A. Yoshinaga and J. Harada, *Jpn. J. Appl. Phys.* **32**, 1191 (1993).
14. S. S. Laderman, A. Fischer-Colbrie, A. Shimazaki, K. Miyazaki, S. Brennan, N. Takaura, P. Pianetta and J. B. Kortright, *Adv. X-Ray Chem. Anal. Jpn.* **26s**, 91 (1995).
15. UC Standardization Committee, *Ultra Clean Technol.* **8**, 44 (1996).
16. N. Streckfuß, L. Frey, G. Zielonka, F. Kroninger, C. Ryzlewicz and H. Ryssel, *Fresenius' J. Anal. Chem.* **343**, 765 (1992).
17. Y. Mori and K. Shimanoe, *Anal. Sci.* **12**, 277 (1996).
18. R. Keller, M. Deicher, W. Pfeiffer, H. Skudlik, D. Steiner and Th. Wichert, *Phys. Rev. Lett.* **65**, 2023 (1990).
19. T. Utaka, Y. Sako, S. Kojima, K. Iwamoto, H. Kouno and J. Atsumi, *Adv. X-Ray Chem. Anal. Jpn.* **23**, 225 (1992).
20. K. Yakushiji, S. Ohkawa, A. Yoshinaga and J. Harada, *Anal. Sci.* **11**, 505 (1995).
21. M. Funabashi, T. Utaka and T. Arai, *Spectrochim. Acta, Part B* **52**, 887 (1997).
22. T. Yamada, T. Shoji, M. Funabashi, T. Utaka, W. Arai and R. Wilson, *Adv. X-Ray Chem. Anal. Jpn.* **26s**, 53 (1995).